Solar Powered 10 mg Silicon Robot

Seth Hollar[1], Anita Flynn[2], Colby Bellew[3] and K.S.J. Pister[1]

Berkeley Sensor and Actuator Center, University of California, Berkeley 94720[1]
MicroPropulsion Corporation, Oakland, CA 94606[2]
Molecular Reflections, San Diego, CA 92121[3]

ABSTRACT

We have demonstrated an autonomous two-legged microrobot which has taken its first steps. The body of the robot is fabricated in a planarized silicon-on-insulator (SOI), two-layer polysilicon process and is 8.5 mm x 4 mm x 0.5 mm in size. We previously reported initial leg motion from an off-board controller but have now incorporated control and power supplies onto the robot, resulting in autonomous operation for the first time. This solar-powered microrobot has two, one degree-of-freedom (DOF) legs and drags its tail end. Leg motion is generated via electrostatic inchworm motors on the robot body. The robot is a three chip hybrid assembled from one chip which contains the robot's motors and legs, a second chip which integrates both solar cells and high voltage buffers, and a third chip which incorporates CMOS circuitry for sequencing the legs. The robot has demonstrated 3 mm of motion shuffling sideways and has lifted its front end more than 300 μm above the surface. The total weight of the three-chip robot is only 10.2 mg.

1. INTRODUCTION

Our main goal was to build an untethered walking microrobot. Until now, microrobots had been powered by off-board power sources, either through wires, vibration, or electromagnetic waves [1-4]. Our strategy, however, was to focus on power consumption, designing the robot around a renewable and plentiful source of energy, the sun.

When we began, there was not a known "process" or manufacturing scheme that would allow one to build microrobots. While a unified process that combined electronics and MEMS together seemed appealing at first glance, the time and energy required for such a development would have been more appropriate for a large company than a small group of researchers. Therefore, we focused on reliable processes when possible and innovated on others when necessary. Breaking down this difficult task into three processes allowed us to manage complexity while maintaining freedom of design.

2. DESIGN

We decided to decompose the problem into three facets: control, power, and mechanical motion. Figure 1 shows the final robot. The digital sequencer (control) was fabricated by National Semiconductor Corporation in their 0.25 μm, 5 metal layer process. We chose to put solar cells (power) and high-voltage buffers on one SOI substrate. SOI wafers gave us the ability to stack solar cells in series and isolate transistors. This technology was based on Bellew's work [5] and has been adapted here using 15 μm thick SOI
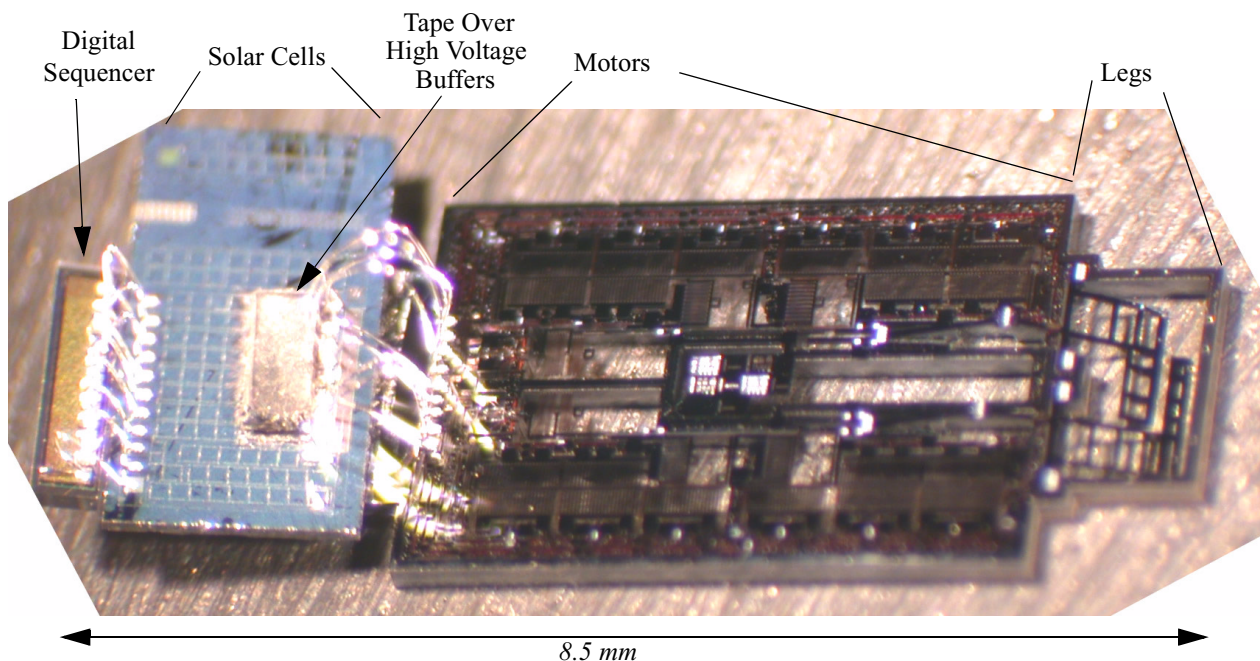
Figure 1. Three-chip working robot. The digital sequencer outputs 3.2 V signals which are converted to 50 V on the solar-cell/high-voltage-buffer chip and sent to the robot chip to drive the electrostatic inchworm motors. The motors drive the legs via rigid links and pin-joint hinges to lift up the robot.
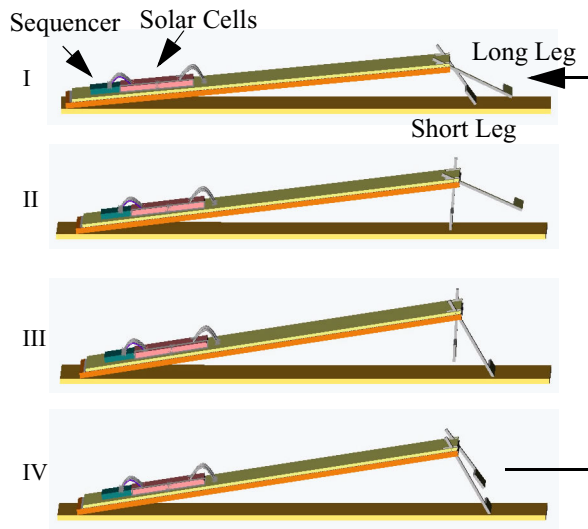
Figure 2. Leg sequence for walking robot. I) Short leg rests on ground. II) Short leg actuates and pulls robot forward. III) Long leg actuates, lifting short leg off ground. IV) Short leg retracts to nominal position. Long leg then retracts bringing the cycle back to step I.

to create 90 cells connected in series for a 50 V supply. We also chose SOI wafers for a separate process for designing motors and legs (mechanical motion). This gave us the ability to do both front and backside etches easily to reduce the weight of the robot's body. The robot motors and legs were previously reported in [6] using a planarized SOI, two-layer polysilicon process. Final assembly was minimal.

2.1 Robot Walking Sequence

To enable walking, two, one-DOF legs are used to move the robot forward. As illustrated in Figure 2, the legs go through four steps to complete a single forward cycle. The robot starts in step I with the short leg touching the ground. In step II, the short leg actuates through 30° of motion, pulling the robot forward by 230 µm. In step III, the long leg actuates, sweeping through a larger angle than the short leg, 35°. Towards the end of the cycle, the long leg lifts the short leg from the ground. In step IV, the short leg, no longer on the ground, retracts to the nominal position. Finally, the cycle repeats itself when the long leg retracts, bringing the sequence back to step I. If the legs do not slip on the ground, the overall forward progress per step is 97 µm, as the robot moves backwards in step IV.

2.2 Leg Design

The chip containing the motors and legs of the robot was processed in our planarized SOI/2-poly process in the Berkeley Microfabrication Facility. The process, utilizing only five masks, enables high force actuators from bulk micromachining to be combined with hinges and flexures from surface micromachining [6]. A backside mask is used to pattern areas to be etched away from the SOI wafer's backside to lighten the robot and prevent stiction. A cross section of the process after release is given in Figure 3.

In designing our robot, we confined ourselves to first order estimates of power, mass, and force. Our main concern was the generation of enough force to overcome the weight of the robot. Inchworm motors were chosen because they are extremely efficient and exhibit large force with large displacement. Figure 4 illustrates how each leg is driven by one inchworm motor. The inchworm motor consists of a shuttle which is "inched" along by two pawls, each driven by a clutch-drive pair of GCA arrays [7].

Figure 4 shows the actual layout of a motor-leg pair. Three sets of hinges link the shuttle of the motor to the foot of the robot. Preset structures behind the shuttle are used to increase mechanical advantage during actuation. Additionally, polysilicon flaps constrain the motion of the shuttle to lie in the plane of the inchworm motors.

The motors were originally designed for an SOI device layer thickness of 20 µm. Ultimately though, the process was run with a 45 µm thick SOI device layer.

In our earlier work [6], we had problems with the electrostatic fingers of the clutch array shorting out, preventing the shuttle from functioning reliably. We have since redesigned the clutch actuator allowing adequate space between the fingers and now have reliable shuttle motion.

2.3 Sequencer Design

The sequencer generates the signals used to operate the motors. Since the operation of each of the GCA arrays is strictly binary, the voltage signals generated are simply digital signals.

The sequencer has three basic functional blocks: 1) clock oscillator, 2) logic to generate the walking sequence and 3) voltage translators which convert the 1 V signals used internally to 3 V output levels.

The clock source for the sequencer is composed of an oscillator along with a current reference. A current-starved ring oscillator design was borrowed from Warneke [9]. A low-power current reference, based on [10], used weak inversion concepts to limit the sequencer's total power to 26 nW.

As mentioned previously, the robot goes through 4 steps to complete a full walking cycle. During two transitions (between I->II and II->III), the sequencer generates the signals used to operate the inchworm motors through 64 cycles (shuttle travel of 256 µm). During the other transitions, springs behind the shuttle retract the legs passively.
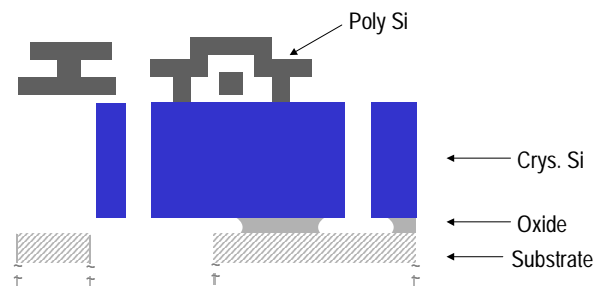
Figure 3. Cross section of the planarized SOI/2-poly process. The process combines high force actuators with polysilicon hinges.
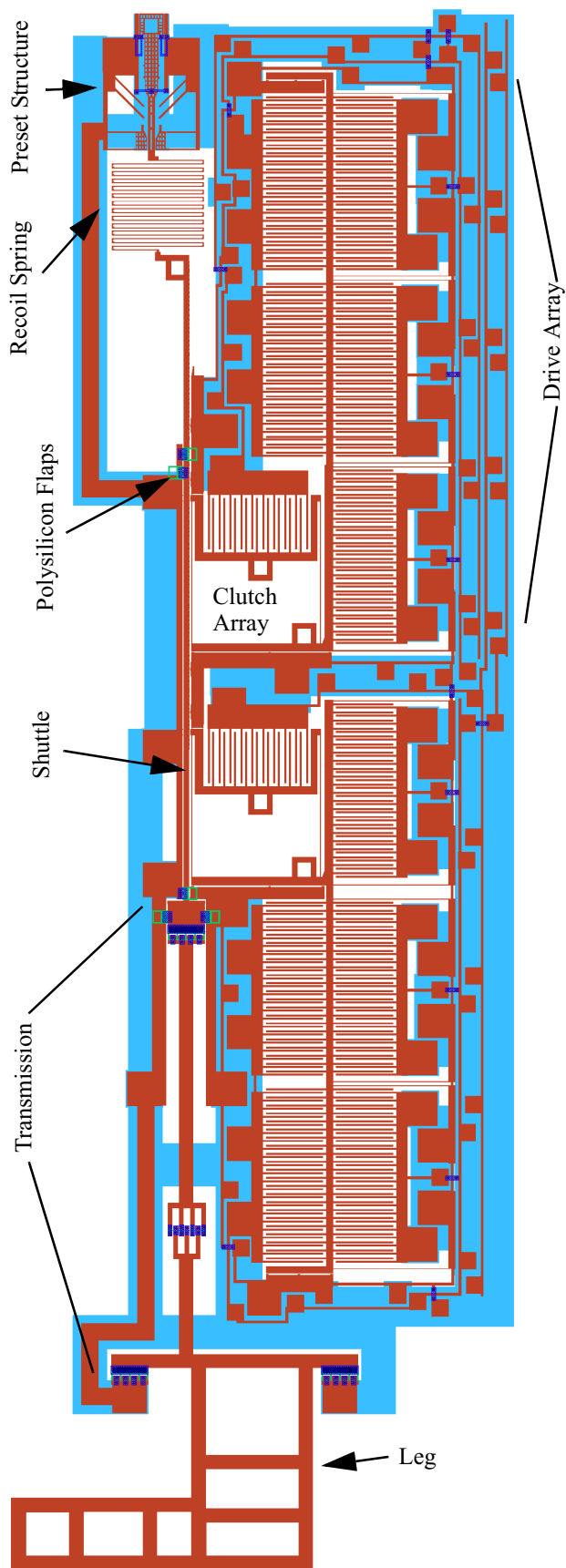
Figure 4. CAD drawing of single leg and inchworm motor of the robot.
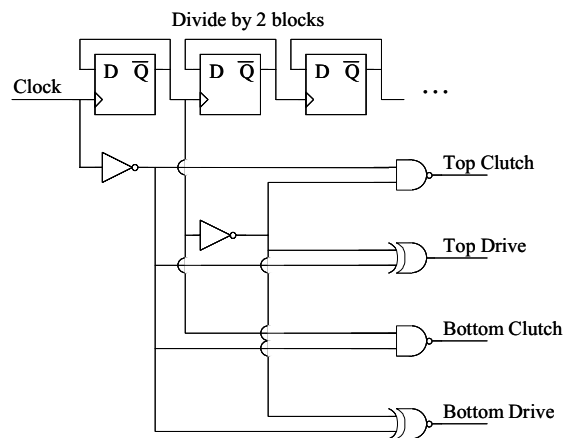
Figure 5. Logic blocks and flip flops used to generate the digital signals for the operation of the inchworm motor.

Figure 5 shows a simplified logic diagram of the sequencer circuit.

While the sequencer operates on a 1 V power supply, it has a second power supply that is also created by the solar cells (~3.2 V). This second supply is used to provide for level shifting so that the output levels will be compatible with the input requirements of the high-voltage buffers on the solar-cell chip. This 3 V intermediate voltage is sufficiently above the threshold voltage of the high-voltage buffers on the solar cell chip, and safely below the breakdown voltage of the devices on the sequencer chip.

As a last note, circuits exposed to light can exhibit relatively large leakage currents. This occurs due to light-generated minority carriers crossing pn junctions of the transistors. Therefore, we use the top-most metal layer, not as a routing layer, but as a light block, to reduce total leakage current.

2.4 Solar Cells and High Voltage Circuits

The chip containing the solar cells and the high voltage transistors was also fabricated in a custom process in the Berkeley Microfabrication Facility. This solar-cell/high-voltage-buffer process is a 7-mask, simplified CMOS process with an eighth mask to define isolation trenches. Originally proposed by Brosnihan *et al.* [11], isolation trenches are used to electrically isolate devices on an SOI wafer. A simplified cross section of our resulting process is found in Figure 6. In all, the process allows one to integrate electrically-isolated MOSFETs along with solar cells onto a common SOI substrate. Dopant parameters and geometry were chosen to yield transistors with moderately high breakdown voltages (~40 V to 50 V for NMOS transistors, 60 V to 100 V for PMOS transistors).

To create the large voltages needed to operate the actuators, 90 solar cells connected in series were fabricated, and then produced an open-circuit voltage above 50 V. With a total effective area of 2 mm^2, the solar cells generated over 100 µW of power under solar illumination.

As described in Section 2.3, the output signals of the sequencer are digital signals with a 3.2 V swing. While
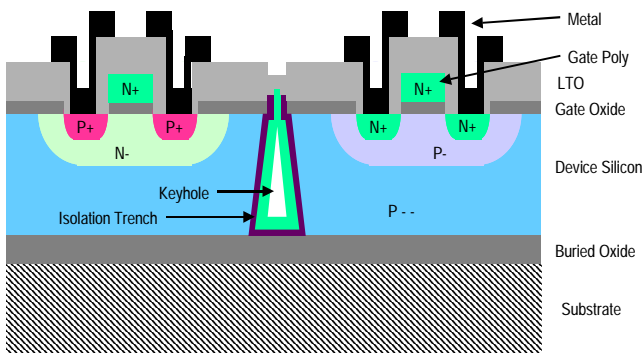
Figure 6. Cross section of solar cell process. Process includes 8 masks. CMOS transistors and solar cells arrays can be co-fabricated in this process.

many methods exist for driving electrostatic actuators (charge/voltage control, adiabatic charging, inductive charging), we chose voltage control for its simplicity and ease of implementation. Ultimately, we designed the voltage translator circuit in Figure 7. The circuit first creates a complimentary signal to the input, $\bar{q}$, and then both q and $\bar{q}$ are fed into a variant of a cross coupled inverter. The circuit requires zero static current to operate. While the output voltage swings from 0 to 50 V, the input voltage only need swing from 0 to 3 V.

Since the solar cell process has only one metal layer, we cannot use it as a light block. Instead, we use black commercial electrical tape diced into rectangles. Using a 5:1 reduced-motion manipulator, we manually placed the tape over the active circuits of the chip. The electrical tape can be seen in Figure 1.

2.5 Assembly of the Three Chip Robot

Once fabricated, the three chips were assembled together and wirebonded. Because the robot had to be able to get up and walk, we had to use assembly methods that did not require permanently fixing the chips to die packages, as is done in traditional wirebonding processes. The assembly sequence followed the three basic steps outlined in Figure 8.
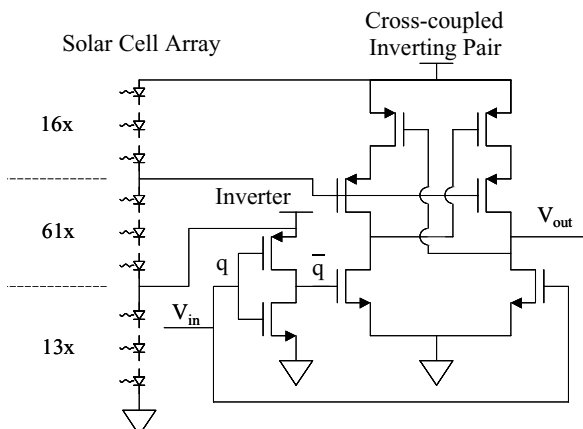
Figure 7. The voltage translator converts the digital signals from the sequencer chip (0 to 3.2 V swing) to voltages needed to run the actuators (0 to 50 V swing). The translator is inverting.
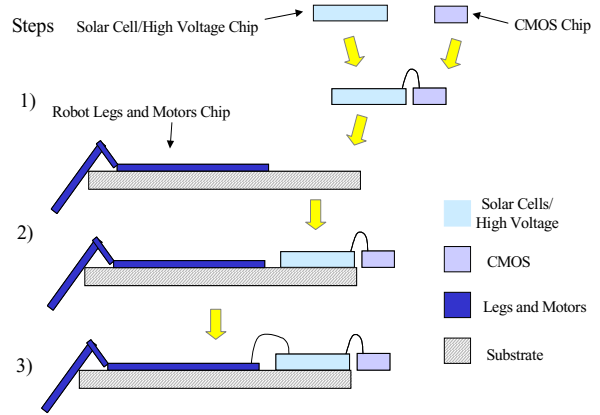
Figure 8. The robot is assembled in 3 steps. 1) Solar cell chip and sequencer are wire bonded together, 2) Solar cell chip is bonded to robot chip with hot wax. 3) Robot and solar cell chip are bonded together.

In the first step, the solar cell chip and sequencer were initially bonded to a handle wafer using Crystalbond mounting wax at 90° C. Once at room temperature, the wax forms a solid bond to the chips. Then the chips are wirebonded together (11 wirebonds) using a Westbond ultrasonic bonder with aluminum wire. After wirebonding, the two chips were subsequently removed from their handle wafer by heating the wax. We verified functionality of the two-chip combination before proceeding to the next step.

The next step entailed bonding the robot chip to a handle wafer with Crystalbond wax similarly to the previous step. This step was a bit more critical because the robot was only 300 µm thick and already released. Care had to be taken to prevent the melted wax from wicking up the sidewalls, breaking hinges. Once the robot was firmly held to its handle wafer, wax was again used to attach the previously wirebonded chips onto the back end of the robot.

Lastly, we wirebonded the high-voltage buffers to the robot (9 wirebonds). To release the robots, we dipped the handle wafer in acetone which dissolved the wax. Afterwards, we rinsed the completed robot in methanol and allowed it to air dry. Since the robots were sufficiently robust, another critical-point-dry was not necessary.

3. EXPERIMENTAL RESULTS

3.1 Sequencer Performance

The sequencer worked nominally at 22 nW. The oscillator frequency was down converted to generate motor cycles on the order of 50 Hz and walking steps a little longer than one second each. However, when the sequencer was illuminated with about one fourth the intensity of the sun, leakage current increased up to 300 µW. At this point, the leakage current starved the current-starved oscillator, preventing it from functioning properly. Future sequencer designs will include an oscillator impervious to light. For our experiments, however, we simply focused a light source on the solar cells but not on the sequencer chip, to the extent that that was possible.
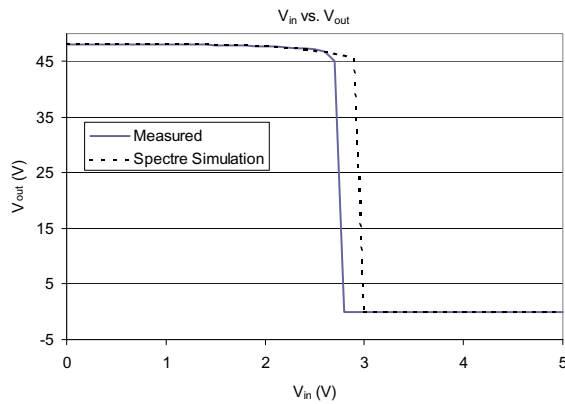
Figure 9. Performance of voltage translator with a 48 V power supply. Simulated results were taken from Spectre using Level 1 models of the transistors.

3.2 Solar Cell and Voltage Translator Performance

The 90-cell solar array generated over 50 V of open circuit voltage. Individual cells, equivalent in size to those used on the robot, 150x150 μm^2, have yielded efficiencies up to 14.3% under AM2.0 illumination.

Threshold voltages from the fabricated transistors fell within 20% of those calculated with Avant! TSuprem-4. Breakdown voltages of the PMOS transistors ranged from 65 V to 100 V, depending on the design. Initially, NMOS transistors exhibited erratic behavior above 42 V. However, repeated measurements at high voltages eventually saw the transistors stabilize themselves with a breakdown voltage above 50 V.

Figure 9 shows plots of the input vs. output voltages of the voltage translators, both measured and simulated. Measurements were taken with an HP 4145 Semiconductor Parameter Analyzer. The DC behavior seemed adequate considering that Level 1 Spice transistor models were used.

Additionally, we both simulated and measured power consumption as a function of frequency for a single voltage translator connected to a robot's clutch actuator (Figure 10). The input voltage swing was 3 V and the output load was modeled with a 1.4 pF capacitance (1.0 pF parasitic capaci-
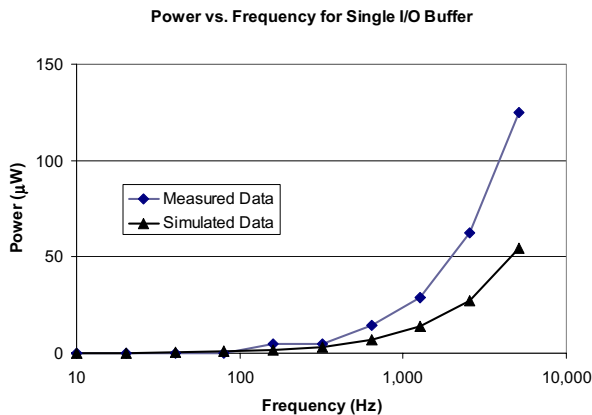
Figure 10. Power consumption vs. frequency of a single voltage translator loaded with a clutch actuator at 50 V. Measured data shows 25 nJ/cycle/actuator, simulated shows 11 nJ/cycle/actuator.
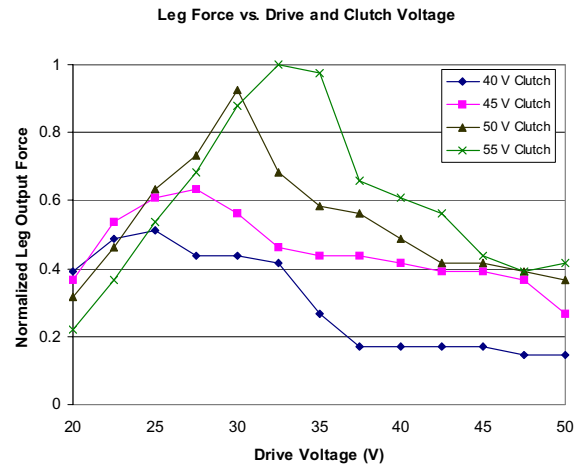
Figure 11. Relative force vs. clutch and drive voltages for long leg.

tance and 0.4 pF load capacitance). Measured data shows that 25 nJ of energy was required to charge and discharge the clutch actuator, yielding a charging efficiency for the system of 1.8%.

About 40% of the power generated from the solar cells is dissipated through leakage current. The power loss occurs from leakage current in the voltage translators due to illumination.

3.3 Leg Performance

With an off-board controller, we have demonstrated both legs working at shuttle speeds of 4 mm/sec, over 100 times, with no failure. Each leg sweeps through 30° of motion yielding an angular rotation rate of 480°/sec. Force measurements were taken with a vernier spring gauge from MEMS Precision Instruments. Force measurements have shown the long leg produces from 30 μN to 60 μN of force with drive and clutch voltages of the inchworm motors being 32 V and 50 V, respectively. The wide measurement range may be due to the low spring constant of the gauge (0.15 μN/μm) which causes the leg to jam on the vernier spring over wide sweeps.

Nevertheless, we were able to map out a relative force space of the long leg for given drive and clutch actuation voltages (Figure 11). The force increases for increasing drive voltages up to a point, and then decreases. As the clutch voltage increases, the peak of the force curve shifts to the right, indicating the peak force is at a larger drive voltage. This pattern indicates that the inchworm motor's clutch is slipping. For low drive voltages, the force the leg can exert is limited by the force the drive actuators can produce. At very high drive voltages the degree of pawl-shuttle slipping increases and thus the leg's output force decreases. As the clutch actuation voltage increases however, the clutch engagement strength increases, increasing the peak force which the leg can exert.

3.4 Robot Performance

Table I shows the measured properties of the robot as a whole. The 10 mg robot's mass is due primarily to the mass

Table I: Robot Properties

	Mass (mg)	Dimensions (μm x μm x μm)	Power Consumed
Motors (+ Legs)	6.4	8611 x 3100 x 300	100 nW
Voltage Translators	(incorporated into solar cell chip)		2.5 μW
Solar Cells	2.3	3600 x 1800 x 150	-100 μW
CMOS Sequencer	0.5	560 x 2050 x 200	22 nW
Robot	10.2	8611 x 3100 x 500	2.6 μW

of the motors and legs. The total power draw of the robot is less than one tenth of the available power from the solar cells in full sunlight.

To date, two fully assembled robots have demonstrated autonomous operation. Using a stereo microscope light, we were able to illuminate the solar cells and observe the legs moving and lifting the robot. With the robot suspended in the air, the legs operated as expected, according to the walking sequence described previously. When placed down on a surface, and running from on-board control and power, the robot was able to lift its own weight. One robot we tested lifted itself up repeatedly with just the short leg working. Without its second leg contributing, it performed one-armed push-ups to a height of over 300 μm above the surface. The other robot lifted itself up with both the short and long legs and went through walking motions for approximately 250 cycles. Instead of going forward however, this robot would slowly veer to the right as its feet slipped on the surface. In one test, the robot shuffled to the right 3 mm over 8 minutes.

4. CONCLUSIONS AND DISCUSSION

Our goal was to build an autonomous microrobot that could get up and walk. In the end, we converged on a three-chip solution. Sending out low-voltage CMOS circuitry for the sequencer to a commercial foundry helped to decompose the complexity of the system into manageable pieces. For mechanical motion, we devised a simple 5-mask process for the motors and legs of the robot. Solar cells provided an easy and convenient means of creating the high voltage levels needed to drive electrostatic actuators. Even though both of our custom processes relied on SOI substrates, we chose
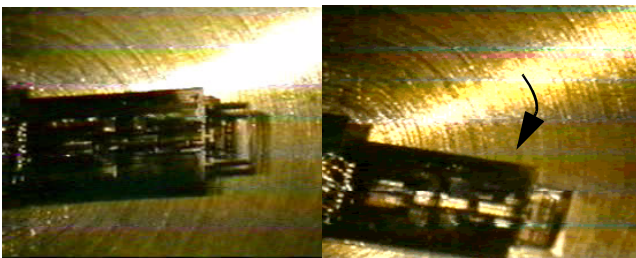
Figure 12. Robot slides to the right about 3 mm over 8 minutes. The surface is machined aluminum.

to develop two separate processes because we could simplify each.

Our robot creation has moved autonomously under its own power, and its legs have exerted enough force to lift the body above the walking surface. Unfortunately, the robot has not yet walked forward. Many improvements can be made on this first design. The low contact friction between the legs and the walking surface prevents the robot from moving forward reliably. In addition, the inchworm motors suffer from pawl-shuttle slippage due to rounding of the engaging teeth during the deep reactive-ion etch. Nonetheless, we have established a firm foundation for launching new designs of microrobots. Multi-DOF legs and joints will be combined with microprocessor-based intelligence, sensors, and communication to create insect-like microrobots. In the not too distant future, we look forward to colonies of robotic ants scurrying about looking for something to do.

REFERENCES

[1] R. Yeh, E. Kruglick and K.S.J. Pister, "Surface-micromachined components for articulated microrobots," *JMEMS*, vol. 5, no. 1, pp. 10-17, 1996.

[2] N. Miki and I. Shimoyama, "Flight performance of micro-wings rotating in an alternating magnetic field," *Technical Digest of MEMS 99*, Orlando, FL, pp. 153-8, 1999.

[3] T. Yasuda, I Shimoyama and H. Miura, "Microrobot locomotion in a mechanical vibration field," *Advanced Robotics*, vol. 9, no. 2, 1995.

[4] T. Ebefors, J. Mattsson, E. Kalvesten and G. Stemme, "A micromotion system based on polyimide joint actuators," *Eurosensors XII*, pp. 391-4, 1998.

[5] C. Bellew, "An SOI process for integrated solar power, circuitry and actuators for autonomous MEMS," *Doctoral Dissertation*, Mechanical Engineering, UC Berkeley, June 2002.

[6] S. Hollar, A. Flynn, S. Bergbreiter and K.S.J. Pister, "Robot leg motion in a planarized SOI/2-poly process," *Proceedings of the Solid-State Sensor, Actuator and Microsystems Workshop*, Hilton Head, SC, June 2002.

[7] R. Yeh, S. Hollar and K.S.J. Pister, "A single mask, large force and large displacement electrostatic inchworm motor," *JMEMS*, vol. 11, no. 4, August 2002.

[8] R. Yeh, "Articulated mechanisms and electrostatic actuators for autonomous microrobots," *Doctoral Dissertation*, Mechanical Engineering, UC Berkeley, June 2001.

[9] B. Warneke, personal communication, June, 2001.

[10] J. Franca and Y. Tsividis, *Design of Analog-Digital VLSI Circuits for Telecommunications and Signal Processing*, Prentice Hall Inc., Englewood, New Jersey, pp.77-8, 1994.

[11] T. Brosnihan, J. Bustillo, A. Pisano and R. Howe, "Embedded interconnect and electrical isolation for high-aspect-ratio, SOI inertial instruments," *Transducers '97*, pp. 637-40, 1997.